Dynamic modelling of cell shape during oscillatory pollen tube growth

Problem presented by

L. J. Winship

at the 5th Mathematics in the Plant Sciences Study Group,
Nottingham 3–6 January, 2012

Contributors

O. Bain, R. J. Dyson, J. Hiorns, J.R. King, A. Korn,
M.R. Nelson, R. O'Dea, S. P. Pearce, A. Smith

March 12, 2013

1 Introduction

The pollen tube is a long, thin cell ($16 - 20\mu$m diameter, up to 4cm length in lily) that grows out of a pollen grain at germination. In fertilization of flowers, the pollen tube plays a crucial role, creating a path through the stile for the sperm nuclei to reach the egg, deep inside the flower. The driving force for tube growth is turgor pressure, generated by a gradient in solutes across the semipermeable cell membrane. The force of turgor pressure is balanced by the tensile strength of the cell wall. Growth occurs due to localized yielding of the wall. The local rate of expansion is a function of local wall properties and is balanced by secretion (exocytosis) of new wall material so that wall thickness and strength are sustained. Maximum expansion rates are found at the tip of the cell, declining to zero some distance behind the tip [4] thus leading to growth exclusively at the tip of the cell. The pollen tube cell wall is mainly composed of pectins, polymers of acidic sugars (primarily galacturonic acid) secreted in an esterified form, with a methyl group covalently bound to each acid

moiety. Pectin Methylesterase (PME) is secreted with the pectins and over time removes the methyl groups creating negative charges that bind calcium entering from the medium. Once cross-linked, pectins are more resistant to tensile stress in the wall. Wall thickness and local expansion rate are thus determined by the balance between the rate of wall thinning, the rate of deposition of new esterified pectins, and the rate of maturation of the pectins as PME cleaves methoxy groups, and calcium ions form crosslinks. We propose that the regulation of localized deposition and the rate of pectin maturation in the tip region are an important part of the mechanism by which pollen tubes control expansion rates and thus pollen tube polarity and directional growth.

In culture and in vivo growth can be very rapid (0.1 to 0.6μm s^{-1}), and typically, in culture, develops a stable oscillatory pattern. The growth rate of lily pollen tubes alternately accelerates and decelerates with a period of 25 to 40 seconds and with high amplitude. These stable oscillations offer a way to unravel the connections between cellular processes, showing both the sequence of events in wall expansion and also the regulatory feedback mechanisms. For example, thickness of the cell wall at the lily pollen tube tip oscillates with the same frequency as does growth rate, shifted earlier in phase by 1/3 of a cycle [2].

Several published models of tip growth have successfully replicated the shape of the tube tip and oscillatory growth, and have incorporated a variety of different feedback mechanisms. In all cases, these models have assumed a self-similar tube shape that does not change during growth. In our hands, oscillating lily pollen tube tips display a distinct pattern of shape change during growth, from oblate to spherical and sometimes all the way to prolate and then back again. We think these shape changes might be used to correlate with measurements of other properties, such as vesicle densities and locations, internal ion gradients, actin density, and propidium iodide staining (related to calcium binding) as a way to understand the regulation of cell wall expansion during tip growth.

Many models of tip growth draw upon the assumptions and mechanics of thin shell theory, considering the pollen tube wall as an elastic or plastic membrane under tensile stress. In the work described here we take the view that cell wall expansion is better described as viscous flow of material in a curved thin shell. Patterns of cell shape and local curvature are derived from the dynamics of viscous flow and dynamic changes in wall properties brought about by expansion, exocytosis of new material and the aging of the new pectins. We assume pressure is isotropic and constant (well substantiated in the literature) so local relative rates of expansion must be solely a function of geometry and wall properties. Using such models we can estimate local stress in the wall from the local curvature, an estimate of thickness (from electron micrographs) and pressure. Each spatial pattern of viscosity should result in a specific shape perhaps ultimately allowing us to infer wall properties from the changes in shape seen in oscillating pollen tubes.

In section 2 we derive a model for the shape of the pollen tube tip, including coupling the viscosity of the wall material to the deposition of new material. In section 3 we then analyse

the model using several different methods. We first neglect this coupling and prescribing the shape and calculating the required changes in one of viscosity, material deposition and thickness given a profile of the remaining two. Continuing to neglect this coupling we then calculate steady state shapes given a viscosity profile, assuming the material deposition is that required to maintain a constant wall thickness. Finally, we solve the full time dependent problem including the viscosity coupling for given profiles of new material deposition. In section 4 we summarise with a brief discussion.

2 Model

2.1 Governing equations

We consider a model of pollen tube growth where we represent the pollen tube wall as a thin sheet of material which is inflated via the internal turgor pressure. The model is formulated in a frame of reference moving with the pollen tube tip; the shaft of the pollen tube which is stationary in the lab frame is thus moving out of the domain of consideration once the material has hardened. This velocity is equivalent to the growth rate of the pollen tube. Since the thickness of the cell wall is significantly less than the radius of the pollen tube we can simplify the analysis by averaging all properties across the thickness of the cell wall. The pollen tube is taken to be axisymmetric. We use an arc length based coordinate system where $s^* = 0$ is at the tip of the pollen tube and $s^* = L^*(t^*)$ is the point at which the wall material no longer expands. (Stars denote dimensional variables.) The location of this point is unknown *a priori*, since is the length of the expanding portion of the cell wall varies temporally. Figure 1 introduces the problem geometry and parameterisation, and Table 1 collates the quantities appearing in the model equations.

By the definition of arc length we require

$$\left(\frac{\partial r^*}{\partial s^*}\right)^2 + \left(\frac{\partial z^*}{\partial s^*}\right)^2 = 1. \tag{1}$$

The axial and azimuthal curvatures are then defined such that

$$\kappa_\theta^* = \frac{1}{r^*}\frac{\partial z^*}{\partial s^*}, \tag{2}$$

$$\kappa_s^* = \frac{\partial^2 z^*}{\partial s^{*2}} \Big/ \frac{\partial r^*}{\partial s^*} = \kappa_\theta^* + r^* \frac{\partial \kappa_\theta^*}{\partial s^*} \Big/ \frac{\partial r^*}{\partial s^*}. \tag{3}$$

Conservation of mass gives [3, 1]

$$\frac{\partial}{\partial t^*}(h^* r^*) + \frac{\partial}{\partial s^*}(u^* h^* r^*) = r^* \eta^*(s,t), \tag{4}$$

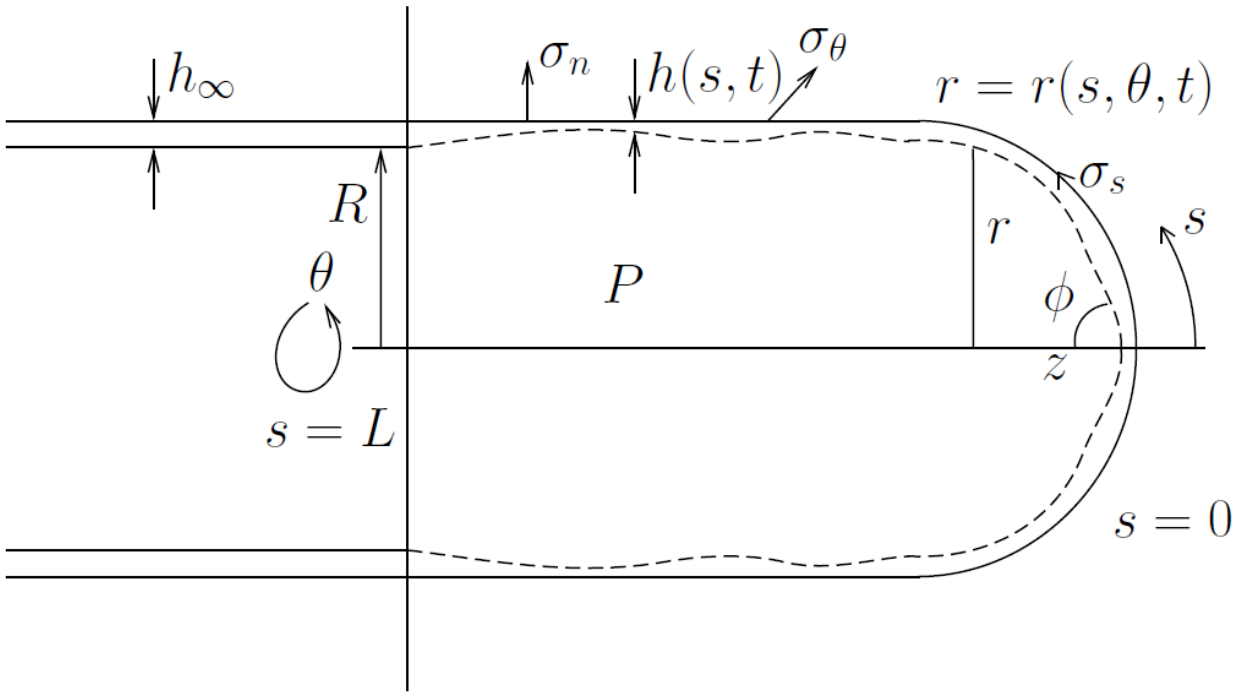

Figure 1: Sketch of the pollen tube growth process.

where we include a source term $\eta(s,t)$ of new material. Conservation of momentum, incorporating an internal pressure P^* leads to

$$\frac{\partial}{\partial s^*}(r^* h^* \sigma_s^*) - \frac{\partial r^*}{\partial s^*} h^* \sigma_\theta^* = 0, \tag{5}$$

$$\kappa_s^* \sigma_s^* + \kappa_\theta^* \sigma_\theta^* = \frac{P^*}{h^*}. \tag{6}$$

These equations hold for any type of material in such a geometry. It remains to specify the material behaviour via appropriate constitutive laws. Plant cell walls typically exhibit viscoelastic behaviour, and on the timescale of growth the viscous behaviour is dominant. We therefore approximate the cell wall material as a viscous fluid. This approximation will become invalid as the cell wall stiffens but will suffice for our purposes. We thus take

$$\sigma_s^* = \frac{2\mu^*}{r^*}\left[2r^*\frac{\partial u^*}{\partial s^*} + \frac{\partial r^*}{\partial t^*} + u^*\frac{\partial r^*}{\partial s^*}\right], \tag{7}$$

$$\sigma_\theta^* = \frac{2\mu^*}{r^*}\left[r^*\frac{\partial u^*}{\partial s^*} + 2\left(\frac{\partial r^*}{\partial t^*} + u^*\frac{\partial r^*}{\partial s^*}\right)\right] \tag{8}$$

where μ^* is the cell wall viscosity and u^* is the meridional velocity [5]. These expressions give the averaged stresses across the thickness of the cell wall. The viscosity of the pectin which

Table 1: Model quantities of the pollen tube growth process.

indep. var.	description	order of magnitude
s^*	arc length	5 μm
t^*	time	500 s
dep. var.		
L^*	upper limit of arc length	15 μm
h^*	cell wall thickness	1 μm
r^*	cell radius	5 μm
z^*	axial distance from tip	5 μm
u^*	cell wall material velocity along s	0.5 μm/s
$\sigma_\theta^*, \sigma_s^*$	principal stresses	3 MPa
$\kappa_\theta^*, \kappa_s^*$	principal curvatures	0.1 μm^{-1}
$\mu^*(s^*, t^*)$	wall viscosity	200 MPa · s
parameters		
P^*	turgor pressure	300 kPa
r_∞^*	shank radius (far from tip)	10 μm
h_∞^*	shank cell wall thickness (far from tip)	1 μm
$\Gamma^*(t^*)$	tip growth rate (axial direction)	0.3 μm/s
$\eta^*(s^*, t^*)$	wall deposition rate	0.1 s^{-1}?
λ^*	rate of stiffening of material via enzyme action	

make up the cell wall evolves in time due to the action of pectinmethylesterase enzymes which increase the viscosity of the pectin. However, new material is also being deposited into the cell wall at rate $\eta^*(s,t)$. This new material is deposited with an initial viscosity lower than that of the composite wall it is being introduced into since it has not yet been stiffened. This results in a lowering of the effective averaged viscosity of the cell wall. Therefore we assume the thickness-averaged viscosity of the cell wall $\mu^*(s,t)$ satisfies

$$\frac{\partial}{\partial t^*}\left(\mu^* h^* r^*\right) + \frac{\partial}{\partial s^*}\left(\mu^* h^* r^* u^*\right) \;=\; \mu_0^* r^* \eta^* + \lambda^* \mu^* r^* h^*, \tag{9}$$

where the first term on the right hand side represents the reduction in viscosity due to the incorporation of new material at lower viscosity (μ_0^*) and the second term represents a stiffening of the material in time via enzyme action (with rate constant λ^*). This becomes

$$\frac{\partial \mu^*}{\partial t^*} + u^* \frac{\partial \mu^*}{\partial s^*} \;=\; -\left(\mu^* - \mu_0^*\right)\frac{\eta^*}{h^*} + \lambda^* \mu^*. \tag{10}$$

We prescribe $u^* = 0$, $r^* = 0$, $z^* = 0$ along with symmetry conditions $\frac{\partial h^*}{\partial s^*} = 0$, $\frac{\partial z^*}{\partial s^*} = 0$, $\frac{\partial \mu^*}{\partial s^*} = 0$ at $s^* = 0$. The point at which the growing pollen tube tip transitions to the rigid shaft is defined to occur when the averaged viscosity reaches a critical viscosity threshold, *i.e.* $s^* = L^*(t^*)$ is defined by where $\mu^* = \mu_c^*$. To keep σ_θ^* finite at this point (since μ_c^* is in

effect infinity) we require

$$r^* \frac{\partial u^*}{\partial s^*} + 2\left(\frac{\partial r^*}{\partial t^*} + u^* \frac{\partial r^*}{\partial s^*}\right) \quad = \quad 0, \tag{11}$$

at $s^* = L^*(t^*)$ (i.e. zero strain rate).

Finally, we prescribe the initial conditions

$$h^*(s^*, 0) = h^*_\infty, \quad r^*(s^*, 0) = \frac{2l^*_0}{\pi} \sin\left(\frac{\pi s^*}{2l^*_0}\right), \quad \mu^* = \mu_0\left(s^*\right), \tag{12}$$

so the pollen tube is initially an appropriately normalised half dome.

The model will produce output quantities frequently measured experimentally, that is

$$u^*(L^*, t^*) = \Gamma^*(t^*), \quad r^*(L^*, t^*) = r^*_\infty, \quad h^*(L^*, t^*) = h^*_\infty, \tag{13}$$

where Γ^* is the growth rate of the pollen tube, r^*_∞ is the radius of the shaft and h^*_∞ is the thickness of the cell wall in the shaft as well as predicting the profile of the tube.

2.2 Non-dimensionalisation

We nondimensionalise the governing equations above by introducing the following scalings:

$$r^* = L^*_0 r, \qquad s^* = L^*_0 s, \qquad z^* = L^*_0 z, \qquad L^* = L^*_0 L \tag{14a}$$

$$h^* = h^*_\infty h, \qquad t^* = \frac{L^*_0}{\Gamma^*_0} t, \qquad u^* = \Gamma^*_0 u, \tag{14b}$$

$$\eta^* = \frac{h^*_0 \Gamma^*_0}{L^*_0}\eta, \qquad \mu^* = \mu^*_0(0)\mu, \qquad \kappa^*_s = \frac{1}{L^*_0}\kappa_s, \quad \kappa^*_\theta = \frac{1}{L^*_0}\kappa_\theta, \tag{14c}$$

$$\sigma^*_s = \frac{\mu^*_0(0)\Gamma^*_0}{L^*_0}\sigma_s, \qquad \sigma^*_\theta = \frac{\mu_0(0)^*\Gamma^*_0}{L^*_0}\sigma_\theta, \qquad P^* = \frac{\varepsilon\mu^*_0(0)\Gamma^*_0}{L^*_0}P, \tag{14d}$$

where $\varepsilon = \frac{h^*_\infty}{L^*_0}$ gives the aspect ratio of the cell wall and $\Gamma^*_0 = \Gamma^*(0)$. Under these rescalings, equations (1–8) and (10) become

$$\left(\frac{\partial r}{\partial s}\right)^2 + \left(\frac{\partial z}{\partial s}\right)^2 = 1, \tag{15a}$$

$$\kappa_\theta = \frac{1}{r}\frac{\partial z}{\partial s}, \tag{15b}$$

$$\kappa_s = \frac{\partial^2 z}{\partial s^2} \Big/ \frac{\partial r}{\partial s} = \kappa_\theta + r\frac{\partial \kappa_\theta}{\partial s} \Big/ \frac{\partial r}{\partial s}, \tag{15c}$$

$$\frac{\partial}{\partial t}(hr) + \frac{\partial}{\partial s}(uhr) = r\eta, \tag{15d}$$

$$\frac{\partial}{\partial s}(rh\sigma_s) - \frac{\partial r}{\partial s}h\sigma_\theta = 0, \tag{15e}$$

$$\kappa_s\sigma_s + \kappa_\theta\sigma_\theta = \frac{P}{h}, \tag{15f}$$

$$\sigma_s = \frac{2\mu}{r}\left[2r\frac{\partial u}{\partial s} + \frac{\partial r}{\partial t} + u\frac{\partial r}{\partial s}\right], \tag{15g}$$

$$\sigma_\theta = \frac{2\mu}{r}\left[r\frac{\partial u}{\partial s} + 2\left(\frac{\partial r}{\partial t} + u\frac{\partial r}{\partial s}\right)\right], \tag{15h}$$

$$\frac{\partial \mu}{\partial t} + u\frac{\partial \mu}{\partial s} = (\mu_0 - \mu)\frac{\eta}{h} + \lambda\mu, \tag{15i}$$

where $\lambda = \lambda^* L_0^*/\Gamma_0^*$ gives the ratio of wall hardening time to the transit time of material through the system. The system given by (15) is solved subject to boundary conditions given by

$$u = r = z = \frac{\partial h}{\partial s} = \frac{\partial z}{\partial s} = \frac{\partial \mu}{\partial s} = 0 \text{ at } s = 0, \tag{16a}$$

$$r\frac{\partial u}{\partial s} + 2\left(\frac{\partial r}{\partial t} + u\frac{\partial r}{\partial s}\right) = 0 \text{ at } s = L, \tag{16b}$$

and initial conditions given by

$$h(s,0) = 1, \qquad r(s,0) = \frac{2}{\pi}\sin\left(\frac{\pi s}{2}\right), \quad \mu = \mu_0(s), \tag{17}$$

where $\mu_0(s) = \mu_0^*(s^*)/\mu_0^*(0)$.

2.3 Alternative system for numerical computation

Alternatively, the system given by (15) can be expressed in terms of the angle ϕ between the normal to the wall and the z-axis. In this notation, (15) becomes:

$$\frac{\partial r}{\partial s} = \cos\phi, \tag{18a}$$

$$\frac{\partial \phi}{\partial s} = \kappa, \tag{18b}$$

$$\frac{\partial u}{\partial s} = \frac{Pr^2\kappa}{12\mu h\sin^2\phi}, \tag{18c}$$

$$\frac{\mathrm{D}r}{\mathrm{D}t} = \frac{Pr^2\kappa}{12\mu h\sin\phi}\left(3 - \frac{2r\kappa}{\sin\phi}\right), \tag{18d}$$

$$\frac{\partial}{\partial t}(hr) + \frac{\partial}{\partial s}(uhr) = r\eta, \tag{18e}$$

$$\frac{\partial \mu}{\partial t} + u\frac{\partial \mu}{\partial s} = -\left(\mu - \mu_0\right)\frac{\eta}{h} + \lambda\mu, \tag{18f}$$

in which κ is equivalent to κ_s above. (Subscript omitted for brevity.) This system is fifth-order in space; appropriate boundary conditions are

$$u = 0, \qquad r = 0, \qquad \frac{\partial h}{\partial s} = 0 \qquad \text{on } s = 0, \tag{19a}$$

$$\phi = \frac{\pi}{2}, \qquad \frac{\partial u}{\partial s} = 0, \quad \mu = \mu_c \qquad \text{on } s = L, \tag{19b}$$

and initial conditions

$$h(s,0) = 1, \quad r(s,0) = \frac{2}{\pi}\sin\left(\frac{\pi s}{2}\right), \quad \mu = \hat{\mu}(s) \tag{20}$$

3 Solutions to the model

Caveat: Variables are dimensional in some of the following sections!

3.1 Steady state solutions for a hemispherical tip

We first assume the steady-state shape of the pollen tube tip to be a hemisphere, and fix two of μ^*, h^* and η^* before calculating the required profile of the third to give the specified shape. We use the following equations, neglecting the coupling between viscosity and deposition:

$$\kappa_\theta^* = \frac{1}{r^*}\sqrt{1 - \left(\frac{\partial r^*}{\partial s^*}\right)^2}, \tag{21a}$$

$$\frac{\partial u^*}{\partial s^*} = \frac{P^*}{12\mu^* h^* \kappa_\theta^*}\left[1 + \frac{r^*\frac{\partial \kappa_\theta^*}{\partial s^*}}{\kappa_\theta^*\frac{\partial r^*}{\partial s^*}}\right], \tag{21b}$$

$$\frac{\partial r^*}{\partial t^*} + u^*\frac{\partial r^*}{\partial s^*} = \frac{P^* r^*}{12\mu^* h \kappa_\theta^*}\left[1 - 2\frac{r^*\frac{\partial \kappa_\theta^*}{\partial s^*}}{\kappa_\theta^*\frac{\partial r^*}{\partial s^*}}\right], \tag{21c}$$

$$\frac{\partial}{\partial t^*}(h^* r^*) + \frac{\partial}{\partial s^*}(u^* h^* r^*) = r^*\eta^*, \tag{21d}$$

We consider the steady state solution when the tip is a hemisphere, so that $r^* = \sin(\omega^* s^*)/\omega^*$, where $\omega^* = \pi/2L^*$. Equations (21a-21d) reduce to

$$\kappa_\theta^* = \omega^*, \tag{22a}$$

$$\frac{\partial u^*}{\partial s^*} = \frac{P^*}{12\mu^* h^* \omega^*}, \tag{22b}$$

$$u^* = \frac{P^* \tan(\omega^* s^*)}{12\mu^* h^* \omega^{*2}}, \tag{22c}$$

$$\eta^* = \frac{P^*}{12\mu^* \omega^*} \left[2 + \frac{\tan(\omega^* s^*)}{\omega^* h^*} \frac{\partial h^*}{\partial s^*} \right], \tag{22d}$$

We now examine various different cases.

1) Prescribe $\mu^* = \tilde{\mu}^*$ and $h^* = h^*_\infty$. Inputting these values into (22c) and differentiating we find that (22b) is not satisfied for a positive radius. It is therefore not possible to prescribe both the thickness and the viscosity as constants.

2)Prescribe $h^* = h^*_\infty$. In this case we find from (22b) and (22c) that

$$\sec^2(\omega^* s^*) - \frac{\tan(\omega^* s^*)}{\mu^* \omega^*} \frac{\partial \mu^*}{\partial s^*} = 1. \tag{23}$$

For this to be satisfied it is required that

$$\mu^* = \tilde{\mu}^* \sec(\omega^* s^*), \tag{24}$$

where $\tilde{\mu}^*$ is the viscosity at $s^* = 0$. Moving from the tip to the shank, the viscosity tends to infinity. Equations (22c-22d) yield the velocity and the deposition rates, namely

$$u^* = \frac{P^* \sin(\omega^* s^*)}{12\tilde{\mu}^* h^*_\infty \omega^{*2}}, \quad \eta^* = \frac{P^* \cos \omega^* s^*}{6\tilde{\mu}^* \omega^*}. \tag{25}$$

This means that the velocity is zero at $s^* = 0^*$. The deposition rate is maximum at the tip and decreases to zero at the start of the shank.

3)Prescribe $\mu^* = \tilde{\mu}^*$. In this case we find from (22b) and (22c) that

$$\sec^2(\omega^* s^*) - \frac{\tan(\omega^* s^*)}{h^* \omega^*} \frac{\partial h^*}{\partial s^*} = 1. \tag{26}$$

For this to be satisfied it is required that

$$h^* = h^*_0 \sec(\omega^* s^*), \tag{27}$$

where h^*_0 is the thickness at $s^* = 0$. Moving from the tip to the shank, the thickness tends to infinity, so this is unrealistic.

3.2 Steady state solutions for a prescribed viscosity profile

We now calculate the steady-state shape of the pollen tube for different prescribed viscosity profiles $\mu(s)$. We again neglect the coupling between the wall viscosity and the deposition of new material, and further assume we have constant cell wall thickness, $h'(s) = 0$, where the deposition rate, $\eta(s)$, which controls this variation may be solved for subsequently found from equation (15d).

3.2.1 Boundary conditions

Our boundary conditions are specified at $s = 0$, where there exists a coordinate-induced singularity as $r = 0$ at $s = 0$. We therefore need to begin the numerical integration the governing equations at a small distance $\hat{\delta}$ away from s. We therefore introduce the Taylor expansions around $s = 0$ and evaluate at $s = \delta$, giving

$$r(\delta) = r(0) + \delta r'(0) + \mathcal{O}(\delta^2) = \delta r'(0) + \mathcal{O}(\delta^2), \tag{28}$$
$$z'(\delta) = z'(0) + \delta z''(0) + \mathcal{O}(\delta^2) = \delta z''(0) + \mathcal{O}(\delta^2), \tag{29}$$
$$u(\delta) = u(0) + \delta u'(0) + \mathcal{O}(\delta^2) = \delta u'(0) + \mathcal{O}(\delta^2), \tag{30}$$
$$\mu(\delta) = \mu(0) + \delta \mu'(0) + \mathcal{O}(\delta^2) = \mu(0) + \mathcal{O}(\delta^2), \tag{31}$$

where we have used the boundary conditions at $s = 0$. Substituting these expansions into the governing equations and equating the zeroth and first order coefficients of δ we determine the remaining values at $s = 0$ as the solutions to:

$$h(0)\mu(0)r'(0)u''(0) = 0, \tag{32}$$
$$P = \frac{6h(0)\mu(0)z''(0)u'(0)}{r'(0)}, \tag{33}$$
$$r'(0)(\eta(0) - 2h(0)u'(0)) = 0, \tag{34}$$
$$r'(0)^2 = 1 \tag{35}$$
$$\eta(0)(\mu(0) - 1) = \lambda h(0)\mu(0) \tag{36}$$

where we have also assumed that $r''(0) = 0, \eta'(0) = 0$ due to the axisymmetry. Our boundary conditions at zero, which will be applied using the expansions (28), are given by:

$$r'(0) = 1, u''(0) = 0, z''(0) = \frac{P}{12\mu(0)h(0)u'(0)}. \tag{37}$$

A shooting method is then employed with $u'(0)$ being varied in order to satisfy the remaining boundary condition of $\sigma_\theta(1) = 0$.

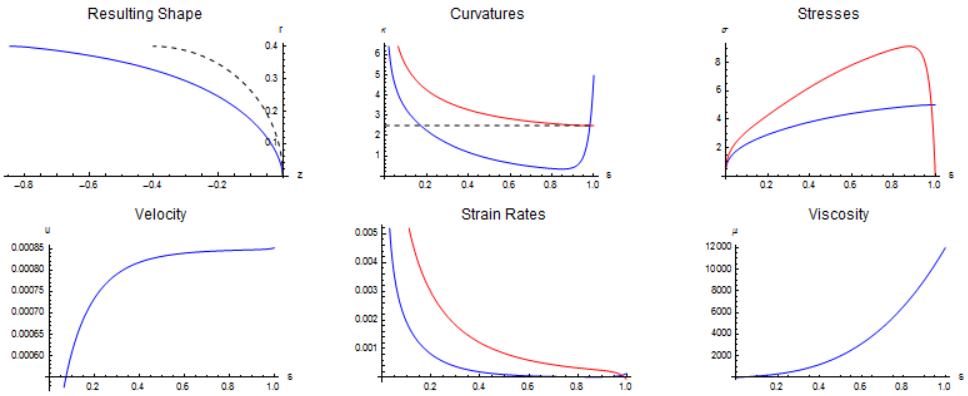

Figure 2: Quantities of interest with the viscosity prescribed as $\mu(s) = 1 + 1000s + 1000s^2 + 10000s^3$, $P = 25$. The dashed line represents the initial condition for the simulations, whilst the red and blues lines (where they appear) represent the θ and s components respectively.

3.2.2 Results

The quantities of interest for a selection of different viscosity functions are given in Figures 2, 3, 4 and 5. It may be seen that changing the spatial dependence of the viscosity induces non-hemispherical steady shapes.

3.3 Numerical solution of the time-dependent problem with viscosity coupling

We now solve the full model incorporating viscosity coupled to deposition, and look at how variations in the profile of deposition affect the evolution of the pollen tube tip shape.

By scaling the arc length, on the (unknown) tip length $L(t)$ via $\hat{s} = s/L(t)$, we simplify the problem domain, and remove the somewhat artificial constraint that $\mu = \mu_c$ defines the point at which the tip becomes the shank; instead, the domain is now $\hat{s} \in [0, 1]$, and we add an explicit equation defining the length $L(t)$ to our system. Note, in the below, we drop carets for brevity.

$$\frac{\partial u}{\partial s} = \frac{LPr^2\kappa}{12\mu h \sin^2\phi}, \tag{38a}$$

$$\frac{\partial r}{\partial t} + \left(\frac{u}{L} - \frac{s}{L}\frac{\mathrm{d}L}{\mathrm{d}t}\right)\frac{\partial r}{\partial s} = \frac{Pr^2}{12\mu h \sin\phi}\left(3 - \frac{2r\kappa}{\sin\phi}\right), \tag{38b}$$

$$\frac{\partial (hr)}{\partial t} + \left(\frac{u}{L} - \frac{s}{L}\frac{\mathrm{d}L}{\mathrm{d}t}\right)\frac{\partial (hr)}{\partial s} = r\eta - \frac{hr}{L}\frac{\partial u}{\partial s}, \tag{38c}$$

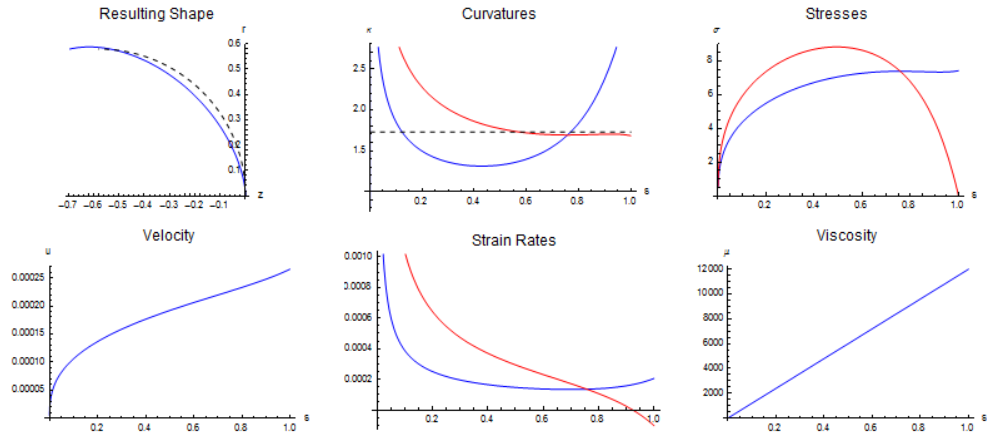

Figure 3: Quantities of interest with the viscosity prescribed as $\mu(s) = 1 + 12000s$,$P = 25$. The dashed line represents the initial condition for the simulations, whilst the red and blues lines (where they appear) represent the θ and s components respectively.

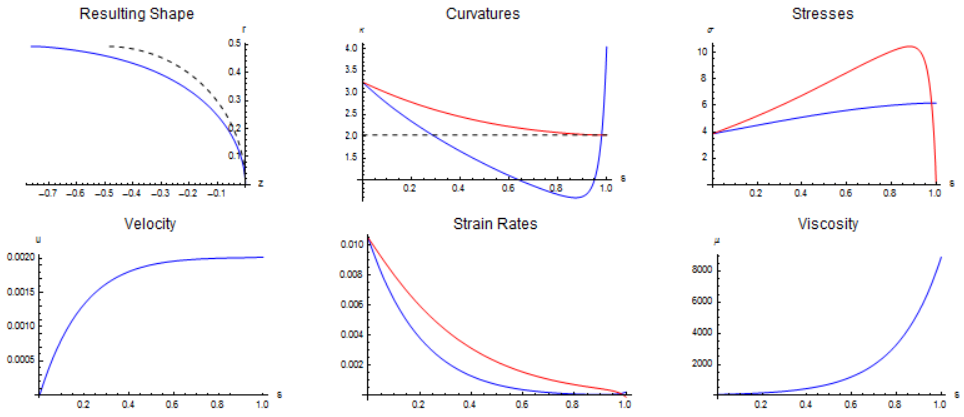

Figure 4: Quantities of interest with the viscosity prescribed as $\mu(s) = 1 + 60e^{5s}$,$P = 25$. The dashed line represents the initial condition for the simulations, whilst the red and blues lines (where they appear) represent the θ and s components respectively.

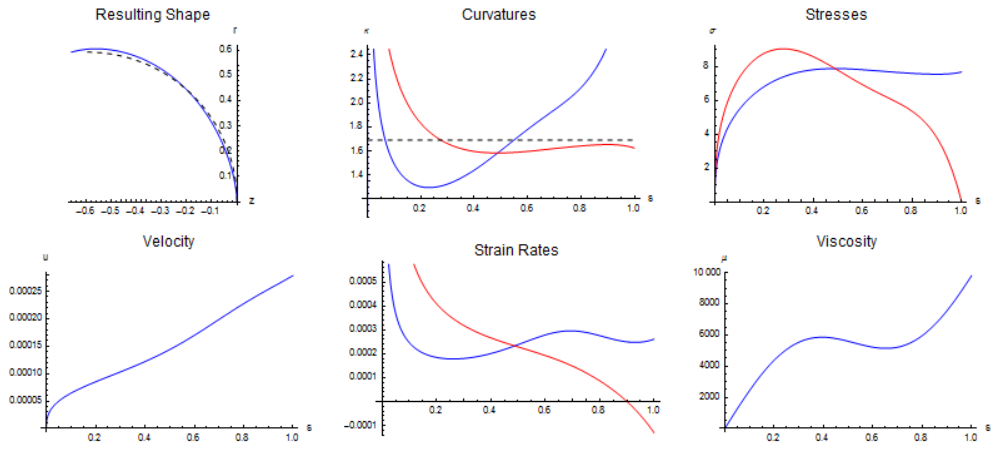

Figure 5: Quantities of interest with the viscosity prescribed as $\mu(s) = 1 + 10500s + 2450\sin(6s)$,$P = 25$. The dashed line represents the initial condition for the simulations, whilst the red and blues lines (where they appear) represent the θ and s components respectively.

$$\frac{\partial \mu}{\partial t} + \left(\frac{u}{L} - \frac{s}{L}\frac{\mathrm{d}L}{\mathrm{d}t}\right)\frac{\partial \mu}{\partial s} = -\eta\frac{\mu - 1}{h} + \lambda\mu, \tag{38d}$$

$$\frac{\mathrm{d}L}{\mathrm{d}t} = u(1,t), \tag{38e}$$

with κ and ϕ obtained via:

$$\phi = \cos^{-1}\left(\frac{1}{L}\frac{\partial r}{\partial s}\right), \qquad \kappa = \frac{1}{L}\frac{\partial \phi}{\partial s}. \tag{39}$$

The system defined by (38) is solved subject to boundary conditions given by

$$r = 0, \qquad u = 0, \qquad \frac{\partial h}{\partial s} = 0, \qquad \text{at } s = 0, \tag{40a}$$

$$\frac{\partial \mu}{\partial s} = 0, \qquad \text{at } s = 1, \tag{40b}$$

and initial conditions given by

$$L(0) = 1, \quad h(s,0) = 1, \quad r(s,0) = \frac{2}{\pi}\sin\left(\frac{\pi s}{2}\right), \quad \mu(s,0) = \hat{\mu}(s). \tag{41}$$

We note that in the numerical simulations that follow, we compare two different choices for the deposition rate $\eta = \eta(s,t)$, corresponding to two main proposed theories for the growth of the pollen tube: (i) that deposition of new material occurs at the tip of the tube; and

(ii) deposition is localised at the 'shoulders' of the growing tube. These mechanisms are encapsulated in the following function

$$\eta(s,t) = \exp(-k(s - La)^2); \tag{42}$$

wherein $a = 0$ defines mechanism (i) and $1 > a > 0$ indicates mechanism (ii). The parameter k determines how localised the deposition is. The location of the shoulder is defined as $s = La$ so that the deposition remains at the same point in the pollen tube despite its growth.

3.3.1 Results

The system (38–39) is solved, subject to the boundary and initial data (40–41), via a second-order finite-difference scheme, together with explicit first-order time-stepping, implemented in MATLAB. An upwind scheme is used for the convective terms in equations (38b–38d): second order backward or forward differences are employed, depending on the sign of $(u/L - s\dot{L}/L)$.

Figure 6 shows a sample simulation, illutrating the evolution of the model variables under deposition mechanism (i); Figure 7 shows the corresponding evolution in the case for which deposition is governed by mechanism (ii). The parameter values are stated in the figure caption.

Figure 6 shows that the tip length of the pollen tube increases slowly over the timescale of the simulation. The dependence of the tip radius on arc length remains unchanged; however, in view of the scaled arc length, this results in a pollen tube whose tip becomes increasingly pointed. The thickness of the pollen tube wall increases at the tip, under the action of deposition, and the viscosity of the wall is correspondingly reduced. The velocity of material moving along the tip wall decreases with time, indicating that the length of the pollen tube will likely reach a steady-state. Figure 7 reveals corresponding behaviour in the case for which the deposition is concentrated on the shoulder of the pollen tube is very similar: the shape of the tube remains unaffected; however, the tube lengthens more slowly due to reduced material velocity, and the position of tube thickening and corresponding viscosity decrease is shifted to the tube shoulder.

In the case of uniform deposition throughout the pollen tube, the qualitative behaviour of the pollen tube is similar to that discussed above; however, the thickening of the tube and its corresponding decrease in viscosity is, of course, uniform throughout the tube. Figure 8 shows simulations corresponding to the choice $\eta = 1$. We remark that in this case, the decrease in lengthening speed is more marked, while the viscosity decrease is reduced.

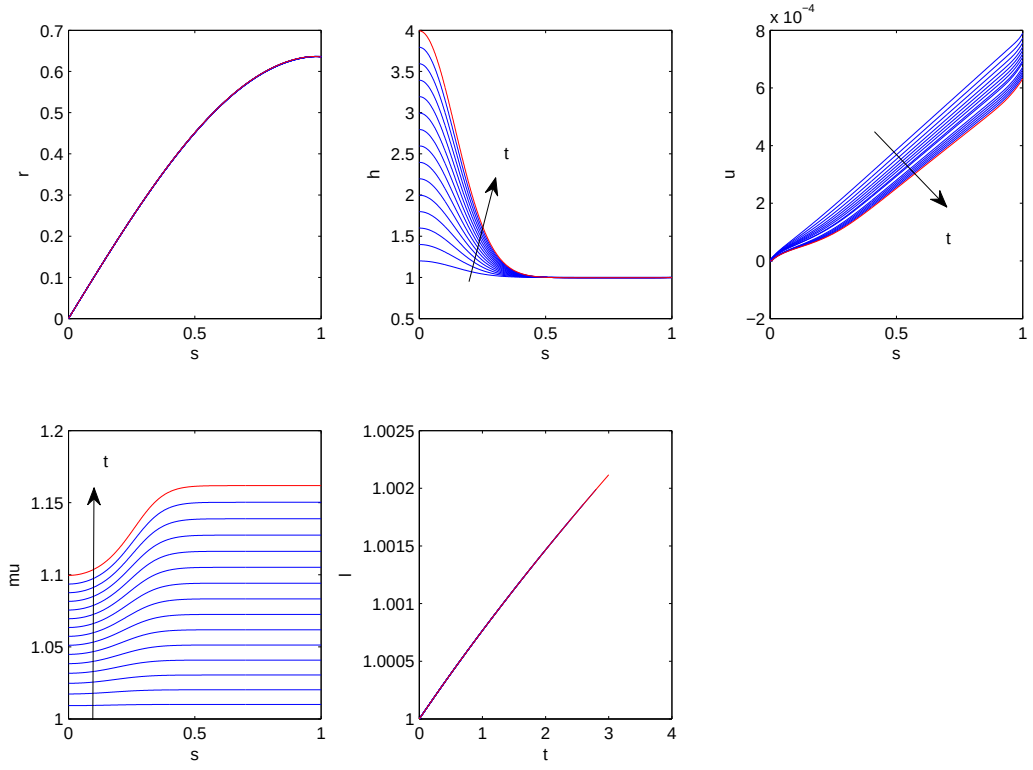

Figure 6: The evolution of the pollen tube radius, thickness, material velocity and viscosity and tube length under the influence of tip deposition. Parameter values are chosen as: $L_0 = 1$, $P = 0.015$, $\lambda = 0.1$, $a = 0$.

4 Discussion and conclusion

We have derived a model of pollen tube growth where we represent the pollen tube wall as a thin sheet of viscous material which is inflated via the (constant) internal turgor pressure. In contrast to previous models, we have explicitly included a coupling between the deposition of new wall material and its viscosity, to model the effect of Pectin Methylesterases stiffening the cell wall material over time. The model has been specified in several different formats within this report to facilitate different analysis methods.

Having derived the model, we first neglected this viscosity coupling and looked for solutions in which the shape of the pollen tube tip was prescribed to be a hemisphere. By fixing two of viscosity, cell wall thickness and deposition rate of new material we calculated the profile of the third required to produce a hemisphere (where this was possible). We then calculated the steady state shape of the pollen tube tip when the thickness was assumed to be constant (and the required deposition to maintain this wall thickness was calculated subsequentally)

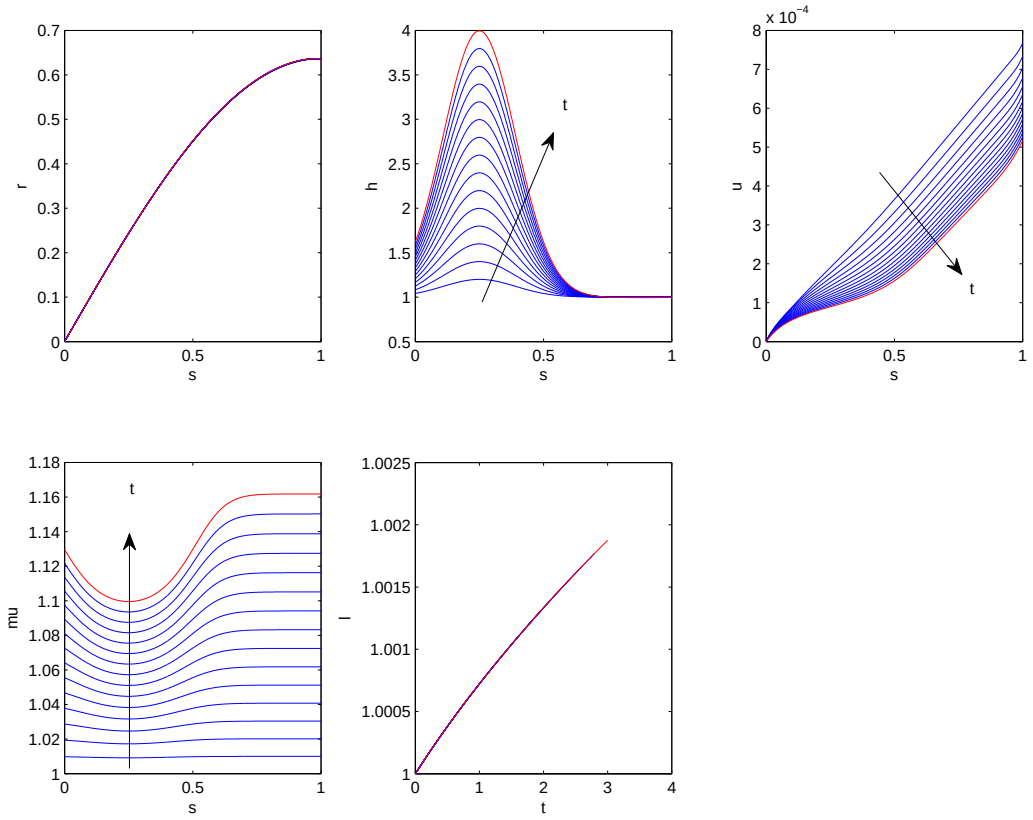

Figure 7: The evolution of the pollen tube radius, thickness, material velocity and viscosity and tube length under the influence of shoulder deposition. Parameter values are chosen as: $L_0 = 1$, $P = 0.015$, $\lambda = 0.1$, $a = 0.25$.

with differing prescribed viscosity profiles. This again neglects the coupling of viscosity and deposition. Finally, we solved the full time dependent problem including viscosity coupling for deposition profiles centred at the tip and shoulder regions of the tube.

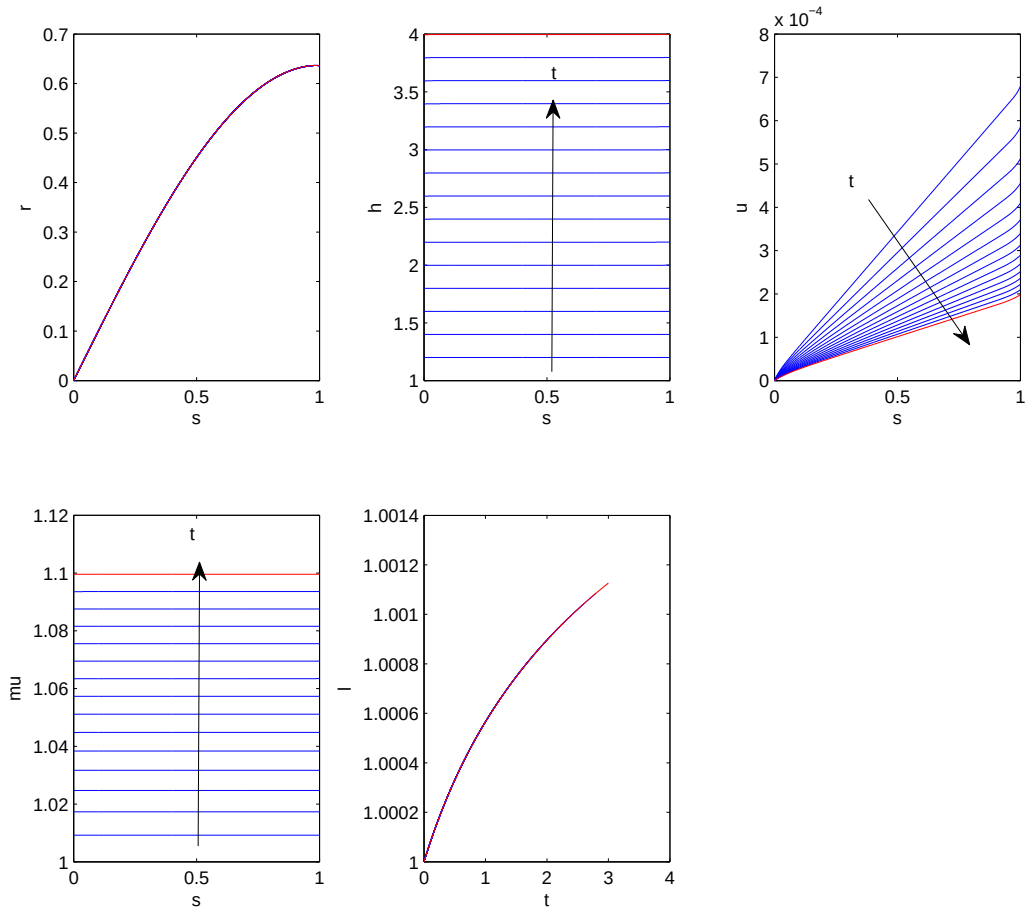

Figure 8: The evolution of the pollen tube radius, thickness, material velocity and viscosity and tube length under the influence of uniform deposition. Parameter values are chosen as: $L = 1$, $P = 0.015$, $\lambda = 0.1$, $\eta = 1$.

References

[1] R. J. Dyson and O. E. Jensen. A fibre-reinforced fluid model of anisotropic plant cell growth. *Journal of Fluid Mechanics*, 655:472–503, 2010. doi: 10.1017/S002211201000100X. URL `http://dx.doi.org/10.1017/S002211201000100X`.

[2] S. McKenna, J. Kunkel, M. Bosch, C. Rounds, L. Vidali, L. Winship, and P. Hepler. Exocytosis precedes and predicts the increase in growth in oscillating pollen tubes. *The Plant Cell Online*, 21(10):3026–3040, 2009.

[3] S. P. Preston, O. E. Jensen, and G. Richardson. Buckling of an axisymmetric vesicle under compression: the effects of resistance to shear. *The Quarterly Journal of Me-*

chanics and Applied Mathematics, 61(1):1–24, 2008. doi: 10.1093/qjmam/hbm021. URL http://qjmam.oxfordjournals.org/content/61/1/1.abstract.

[4] E. Rojas, S. Hotton, and J. Dumais. Chemically mediated mechanical expansion of the pollen tube cell wall. *Biophysical Journal*, 101(8):1844 – 1853, 2011. ISSN 0006-3495. doi: 10.1016/j.bpj.2011.08.016. URL http://www.sciencedirect.com/science/article/pii/S0006349511009623.

[5] B. W. Van De Fliert, P. D. Howell, and J. R. Ockenden. Pressure-driven flow of a thin viscous sheet. *Journal of Fluid Mechanics*, 292:359–376, 1995. doi: 10.1017/S002211209500156X. URL http://dx.doi.org/10.1017/S002211209500156X.